

# Calibration of 2D load for railway embankment stability assessment based on 3D reliability analysis using RFEM

Wei Huang, Michael A. Hicks, Zheng Guan

Department of Geoscience & Engineering, TU Delft, Delft, The Netherlands, W.Huang-1@tudelft.nl

**ABSTRACT:** The Random Finite Element Method (RFEM) is used to calibrate the 2D strip load for the deterministic stability assessment of a railway embankment, considering the effects of 3D train loads and spatial variability of the soil undrained shear strength. 3D random fields are generated to simulate the soil strength variability using different scales of fluctuation in the horizontal plane, and finite element analyses are conducted as part of a Monte Carlo simulation. Each RFEM analysis comprises 500 realizations, from which the probability distribution of undrained bearing capacity is obtained. This allows the 2D design load and resistance to be calibrated against a target reliability level in light of 3D soil spatial variability and load distribution. The results highlight the importance of 3D reliability analysis for the assessment of railway embankments, and the proposed calibration approach provides a reliability-informed 2D solution with improved accuracy.

**KEYWORDS:** Embankment reliability analysis, Random Finite Element Method, 3D soil spatial variability, 2D load calibration.

## 1 INTRODUCTION

In engineering practice, the bearing capacity of railway embankments is generally computed using two-dimensional (2D) plane strain analysis, including simplifications such as homogeneous soil layers and uniform strip loads. However, in reality, soil properties and applied loadings vary in three-dimensional (3D) space, leading to complicated 3D failure mechanisms. Therefore, 3D full probabilistic analysis is desirable to evaluate the reliability of railway embankments, in order to contribute to risk-informed and potentially more cost-effective design and maintenance decisions.

In this study, the design parameters to be used in 2D deterministic analysis are calibrated based on 3D full probabilistic analysis. The Random Finite Element Method (RFEM) (Fenton & Griffiths, 2008) is employed to determine the probabilistic undrained bearing capacity of an idealized railway embankment, considering two key parameters that characterize 3D effects in the system: 1) the length of the surcharge load applied on the embankment in the longitudinal direction, and 2) the horizontal scale of fluctuation that quantifies spatial variability of the soil shear strength. An in-house RFEM code has been developed for this purpose, based on that previously used in 2D (Hicks & Samy, 2002) and 3D (Hicks & Spencer, 2010; Hicks et al., 2014; Hicks & Li, 2018; Varkey et al., 2023) slope reliability analyses. By post-processing the RFEM results for the embankment bearing capacity, the reliability-based calibration of the 2D deterministic design load is demonstrated.

## 2 PROBLEM AND METHODOLOGY

### 2.1 Problem definition

The railway embankment is simplified as a slope loaded by its self-weight and a rectangular uniform surcharge on the top, as illustrated in Figure 1. The slope height of 2 m and the slope angle of 45° are within the typical ranges for railway embankments in the Netherlands, and the distance (in the x-direction) from the nearest edge of the surcharge  $q$  to the slope crest is assumed to be 2 m, which is a reasonable value for the location of the track structure that distributes operational loads over a width of approximately 3 m on the embankment top (CEN, 2021). Note that the dead weight of the track structure has been omitted for simplicity. The length (in the y-direction) of the embankment is set as 100 m, while the surcharge length  $L_q$  is varied (16, 30, 60, 100 m) to simulate different lengths of trains in operation.

### 2.2 Finite element model

In the finite element (FE) model, 20-node hexahedral elements of size 1.0×1.0×0.5 m (in the x-, y-, and z-directions) are adopted, except for along the sloping face where elements have been distorted, and a reduced integration scheme involving 2×2×2 Gauss points in each element is used. The mesh is fully fixed at the base, while the two vertical side faces (in the y-z plane) are constrained only in the x-direction and the two end faces (in the x-z plane) are allowed to move only in the z-direction. Such boundary conditions have been adopted and validated in previous research on 3D slope reliability (Hicks & Spencer, 2010; Hicks et al., 2014).

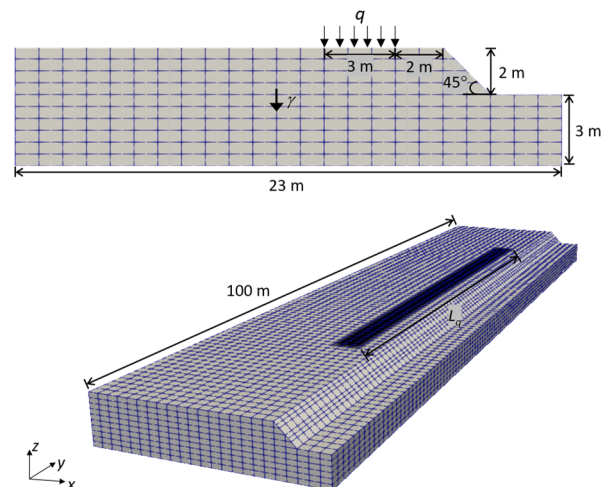


Figure 1. Problem geometry and finite element mesh in 2D and 3D.

Table 1. Soil parameter (mean) values.

Parameter	Symbol	Value	Unit
Unit weight	$\gamma$	20	kN/m <sup>3</sup>
Undrained shear strength	$c_u$	20	kPa
Young's modulus	$E$	$3 \times 10^4$	kPa
Poisson's ratio	$\nu$	0.3	-

The embankment material is modelled using an elastic-perfectly plastic Tresca soil model under undrained (total stress) conditions, and the (mean) values of the relevant parameters are listed in Table 1. By incrementing the magnitude of  $q$  until failure has occurred, signaled by non-convergence after 500

equilibrium iterations, the limit load is taken as the undrained bearing capacity  $q_u$  of the embankment.

### 2.3 RFEM reliability analysis

In RFEM, the stochasticity of a spatially variable soil property is represented by a sufficiently large number of random fields (RFs), for which a variety of generation approaches exist (Fenton & Griffiths, 2008). Here, Local Average Subdivision (LAS) (Fenton & Vanmarcke, 1990) is adopted to discretize the RFs based on the probability density function (PDF) and the spatial correlation function of the material property. To characterize the RFs, the point statistics (i.e., mean and standard deviation), as well as the scales of fluctuation in the different spatial coordinate directions, are needed as input.

The undrained shear strength  $c_u$  is the only stochastic parameter in the current RFEM model. Based on various evidence from laboratory and field test data, as discussed by Hicks and Samy (2002), an underlying normal distribution is assumed for  $c_u$ , along with a spatial correlation structure modeled by a Gauss-Markov correlation function. The normal PDF of  $c_u$  is truncated at a lower threshold of 5 kPa, a typical lower-bound value of  $c_u$  for soft soils in the Netherlands, to avoid negative values, which eliminates less than 0.135% of the possible lower-tail values for relatively low coefficients of variation (i.e.,  $COV < 0.25$ ). The input statistics of  $c_u$  are selected from typical ranges and are listed in Table 2. Multiple values of the horizontal scale of fluctuation are included to investigate its influence on the results, as an accurate estimate is often unavailable due to sparse field data (Phoon, 2023).

Table 2. Point and spatial statistics of  $c_u$ .

Parameter	Symbol	Value	Unit
Mean	$\mu_c$	20	kPa
Standard deviation	$\sigma_c$	4	kPa
Coefficient of variation	$COV_c = \sigma_c / \mu_c$	0.2	-
Horizontal scale of fluctuation (in x & y)	$\theta_h$	4, 8, 16, 30, 60, 120	m
Vertical scale of fluctuation (in z)	$\theta_v$	1	m

Following previous studies (e.g., Hicks et al., 2014), stationary anisotropic RFs are obtained for  $c_u$  by distorting (i.e., squashing in the vertical direction and/or stretching in the horizontal directions to give  $\theta_v < \theta_h$ ) LAS-generated, isotropic, standard normal RFs, and then transforming them to the physical space of  $c_u$  based on  $\mu_c$  and  $\sigma_c$ . These RFs are discretized in such a way that each Gauss point in the FE mesh corresponds to a unique RF cell. A total of 500 RF realizations have been generated for each RFEM analysis, which is sufficient for convergence of the output statistics (i.e., the mean and standard deviation of  $q_u$ ). Subsequently, for a target probability of failure  $P_{f,T}$ , the design load  $q_d$  can be derived from the distribution of  $q_u$  based on the RFEM results, such that

$$P_{f,T} = P(q_u < q_d) \approx \sum_{i=1}^n I(q_u^i < q_d) / n \quad (1)$$

where  $n$  is the total number of realizations,  $q_u^i$  is the value of  $q_u$  from the  $i$ -th realization, and  $I(\bullet)$  is an indicator function equal to 1 if the inequality inside is true or 0 otherwise.

### 2.4 Reliability-based calibration

Based on Equation (1), design load values corresponding to the same  $P_{f,T}$  can be determined and compared across different scenarios, especially with respect to the  $q_d$  obtained from the 2D plane strain analysis that implies  $L_q = \infty$ , for the purpose of

reliability-based design load calibration. To be more specific, let  $q_{d,2D}$  and  $q_{d,3D}$  denote the respective  $q_d$  values derived from 2D and 3D RFEM analyses of the embankment for the same value of  $P_{f,T}$ . Hence, a “load calibration factor”  $\eta_L$  can be defined as the ratio between  $q_{d,2D}$  and  $q_{d,3D}$  in order to convert a limited-length 3D load to a “reliability-equivalent” 2D strip load. This factor is expected to be a function of  $L_q$  and  $\theta_h$ , as well as  $P_{f,T}$ , and is analogous to the load factor in the load and resistance factor design method (Salgado et al., 2011) if considering uncertainty in the 2D load due only to 3D effects of the load length and soil strength variability. Hence,

$$\eta_L = \frac{q_{d,2D}(\theta_h, P_{f,T})}{q_{d,3D}(L_q, \theta_h, P_{f,T})} \text{ or } q_{d,2D} = q_{d,3D} \cdot \eta_L(L_q, \theta_h, P_{f,T}) \quad (2)$$

On the other hand, the resistance (i.e., bearing capacity) in the 2D deterministic design can also be calibrated using a resistance factor  $\eta_R$  that takes into account the uncertainty due to soil spatial variability. In the same context as above, if  $q_{u,det}$  is the deterministic solution obtained for the 2D homogeneous model characterized by the mean strength (i.e.,  $c_u = \mu_c$ ), the design resistance  $q_{u,d}$  benchmarked against the 2D stochastic solution should ensure a probability of failure not exceeding the target one, which, in consistency with Equation (1), gives

$$q_{u,d} = q_{u,det} \cdot \eta_R(\theta_h, P_{f,T}) = q_{d,2D} \text{ or } \eta_R = \frac{q_{d,2D}(\theta_h, P_{f,T})}{q_{u,det}} \quad (3)$$

As such, the calibration factors  $\eta_L$  and  $\eta_R$  derived according to Equations (1)-(3) based on the RFEM results will lead to a reliability-informed 2D deterministic design, where the load  $q_{d,2D}$  and resistance  $q_{u,d}$  have incorporated the effects of 3D load length and soil variability.

## 3 RESULTS AND DISCUSSION

Figure 2 shows typical realizations of spatially variable  $c_u$  in the 3D domain for small and large values of  $\theta_h$  relative to the embankment size. According to the observation of three distinct categories of failure mode for 3D heterogeneous slopes that are loaded by gravity only (Hicks & Spencer, 2010), a smaller  $\theta_h$  results in a higher degree of soil property averaging over potential failure surfaces, whereas a larger  $\theta_h$  indicates the soil has more of a layered status that forces rupture to propagate through horizontally semi-continuous weak zones. Hence, a relatively narrow spread of possible solutions with the mean response closer to the deterministic counterpart is expected for cases with a small  $\theta_h$ . When a surcharge is added on top of the slope, the load length  $L_q$  relative to  $\theta_h$  also plays a role in the probabilistic response, as demonstrated by the histograms in Figure 3 for  $\theta_h = 16$  m. The case of  $L_q = 16$  m yields a similar distribution of  $q_u$  to that from the 2D stochastic model, which can be intuitively explained by potential failures being simultaneously constrained by  $L_q$  and a similar length of semi-continuous weak layers ( $\approx \theta_h$ ) under the loaded area, so tending towards the plane strain condition. In contrast, a much larger  $L_q$  (e.g., 100 m) with respect to  $\theta_h$  enables failure paths to leverage more spatial averaging.

Quantitatively, the probability of failure in these cases for a range of design loads is calculated according to Equation (1) and plotted in Figure 4, which exhibits essentially the cumulative distribution functions derived from the histograms. The curves for the different  $L_q$  values show similar shapes but are offset from each other for  $q_d$  approximately in the range from 40 to 90 kPa, where a larger  $L_q$  is associated with a higher  $P_f$  for a given  $q_d$ , with the 2D (dashed) curve lying amidst the 3D curves and not necessarily giving (un)safely predictions.

Outside the range,  $q_d < 40$  kPa ensures negligibly small  $P_f$ , while  $q_d > 90$  kPa leads to almost certain failure across all cases.

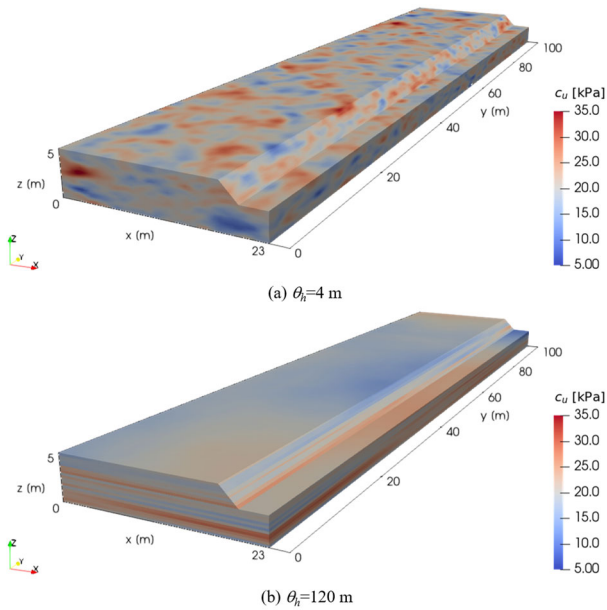


Figure 2. Examples of 3D random fields of  $c_u$  for different  $\theta_h$ .

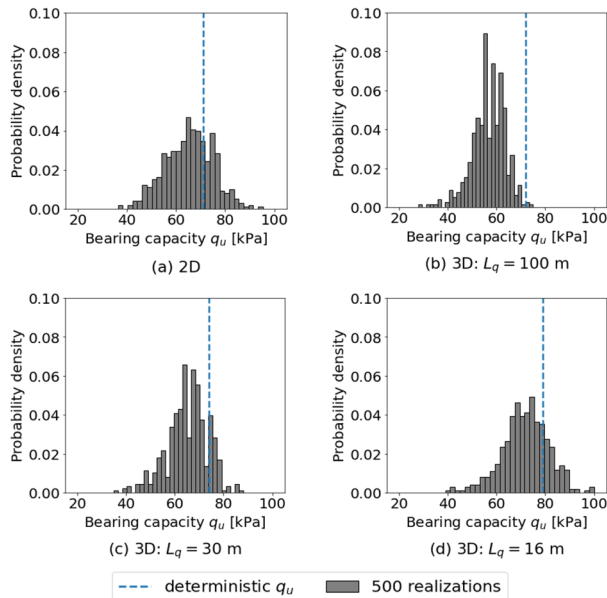


Figure 3. Histograms of  $q_u$  for 2D and 3D cases with  $\theta_h=16$  m.

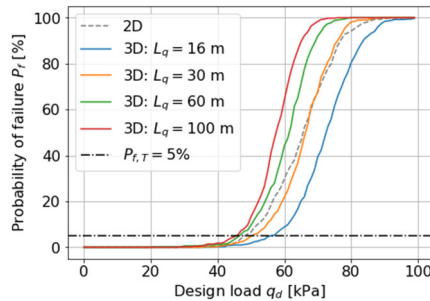


Figure 4. Plots of  $P_f$  vs.  $q_d$  for 2D and 3D cases with  $\theta_h=16$  m.

Drawing a horizontal line representing the value of  $P_{f,T}$ , the intersections of it with the curves in Figure 4 are the reliability-equivalent “design points” that correspond to different  $q_d$  values across the 2D and 3D cases, which are used to calculate the load factor  $\eta_L$  according to Equation (2) as a function of  $L_q$  (as  $\theta_h$  is

fixed). Figure 5 shows the increasing trend of  $\eta_L$  with larger  $L_q$ , for three  $P_{f,T}$  values. It is observed that  $\eta_L \leq 1$  for  $L_q \leq 30$  m, implying an overall higher load-bearing capacity owing to the beneficial 3D effects when  $L_q$  is small relative to the embankment length as well as  $\theta_h$ . In contrast, when  $L_q$  is larger, the relatively small  $\theta_h$  makes it easier for the region under the influence of the load to encompass weak zones that promote semi-continuous or discrete failures, leading to a lower  $q_u$  than under plane strain conditions. Besides, it seems that the critical  $L_q$  at which the 3D load-bearing capacity ceases to be greater than for 2D (i.e., where  $\eta_L = 1$ ) is smaller under a higher reliability requirement (i.e., lower  $P_{f,T}$ ). Thus, it is important to identify the longest maximum load that the embankment is designed to sustain in its service life, and the corresponding load (amplification) factor needs to be applied if a 2D design approach is used.

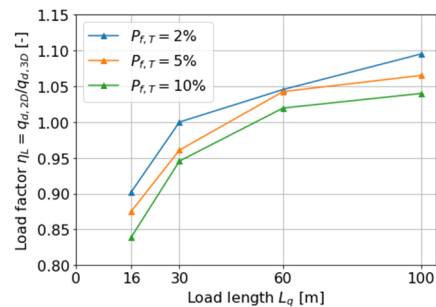


Figure 5. Calibrated  $\eta_L$  vs.  $L_q$  against  $P_{f,T}$  for 3D cases with  $\theta_h=16$  m.

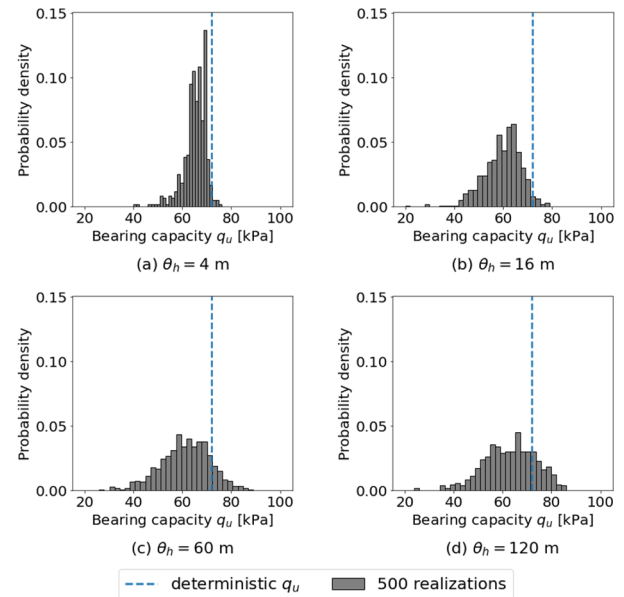


Figure 6. Histograms of  $q_u$  for 3D cases with  $L_q=60$  m.

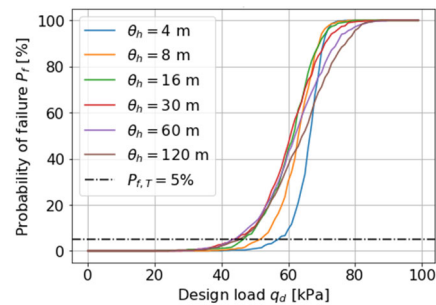


Figure 7. Plots of  $P_f$  vs.  $q_d$  for 3D cases with  $L_q=60$  m.

The same procedure is also applied to cases with the same  $L_q$  value (e.g., 60 m) to study the influence of varying  $\theta_h$ . The

histograms of  $q_u$  displayed in Figure 6 again confirm that a wider range of solutions is possible with a larger  $\theta_h$ . The corresponding cumulative probability curves are shown in Figure 7, and the calibrated load factor against  $P_{f,T}$  as a function of  $\theta_h$  in Figure 8. It is observed that, for a fixed  $L_q$ ,  $\eta_L$  increases with  $\theta_h$  approximately to a point where  $\theta_h \approx L_q$ . The reason for the following slight drop with even larger  $\theta_h$  is not clear and requires further investigation. However,  $\eta_L < 1$  for small  $\theta_h$  is attributed to the spatial averaging effect in the third dimension in the vicinity of the load, while larger  $\theta_h$  favors 3D failure and lowers the overall bearing capacity as it becomes more likely to encounter semi-continuous weak zones in the soil.

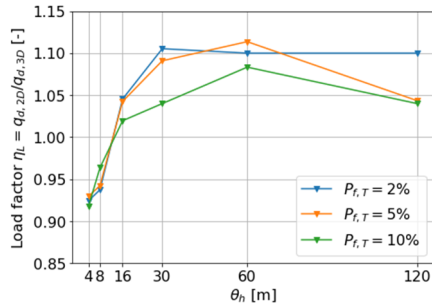


Figure 8. Calibrated  $\eta_L$  vs.  $\theta_h$  against  $P_{f,T}$  for 3D cases with  $L_q=60$  m.

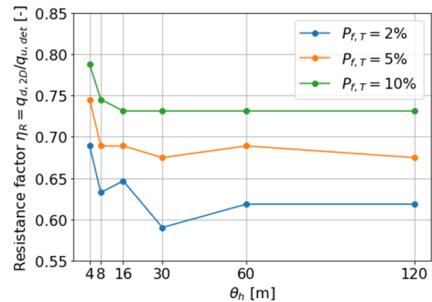


Figure 9. Calibrated  $\eta_R$  vs.  $\theta_h$  against  $P_{f,T}$  for 2D cases.

Aside from transforming the design load from 3D to 2D, the uncertainty in the resistance in a 2D deterministic design also needs to be handled. Using the 2D RFEM results for different  $\theta_h$  values, the reliability-based resistance correction factor  $\eta_R$  is calculated according to Equation (3) and plotted in Figure 9 as a function of  $\theta_h$ . The curves corresponding to different  $P_{f,T}$  values consistently drop and finally flatten with larger  $\theta_h$ , while  $\eta_R < 1$  is always the case. Therefore, to be on the safe side, a very large  $\theta_h$  value, approximately the same as the maximum load length, can be assumed for the calibration of  $\eta_R$  as well as  $\eta_L$ , if no accurate estimate is available.

#### 4 CONCLUSIONS

Surcharge-loaded slopes, such as railway embankments, are subject to uncertainties in a 3D domain, which are usually overlooked in conventional design practice involving only cross-sections and 2D strip loads. In this paper, a series of full probabilistic analyses conducted using RFEM has revealed the impact of 3D soil heterogeneity in conjunction with the out-of-plane load length on the undrained load-bearing capacity of an idealized embankment. Making use of the RFEM results, a practical approach has been proposed for the calibration of 2D load and resistance based on “reliability equivalence”. Major findings include:

1. The 3D effect of a limited load length  $L_q$  and that of the horizontal scale of fluctuation  $\theta_h$  cannot be isolated, as a larger  $L_q$  diminishes the benefits of the end constraints

while a larger  $\theta_h$  leads to a wider spread of solutions, making weak responses more probable. As such, a “worst-case” scenario in 3D for a given (2D) design load can be the maximum  $L_q$  with  $\theta_h \approx L_q$ .

2. The load factor  $\eta_L$ , defined as the ratio of 2D design load to 3D design load for the same target reliability, can be used to calibrate the strip load applied in a plane strain model while reflecting the 3D nature mentioned in point 1. As  $\eta_L$  can be a reduction or amplification factor depending on the combination of  $L_q$  and  $\theta_h$ , the 3D “worst-case” scenario can be taken as a conservative baseline for the load calibration.
3. The resistance factor  $\eta_R$  is a complementary measure that corrects the 2D deterministic bearing capacity based on the same target reliability against which the 2D design load has been calibrated. It is found that  $\eta_R$  is in general a reduction factor, especially when  $\theta_h$  is large.

To conclude, a more comprehensive parametric study involving a diverse range of embankment geometries, load characteristics, and soil properties will help to generalize the findings and contribute to future guidelines for the reliability-based design or assessment of similar geotechnical structures.

#### 5 ACKNOWLEDGEMENTS

This work is part of the research program RESET (“Reliable Embankments for the Safe Expansion of rail Traffic”) funded by ProRail, and has used the Dutch national e-infrastructure with the support of the SURF Cooperative using grant no. EINF-13223. The authors also acknowledge the use of computational resources of the DelftBlue supercomputer, provided by Delft High Performance Computing Centre (<https://www.tudelft.nl/dhpc>).

#### 6 REFERENCES

- CEN, 2021. *NEN-EN 15528 Railway applications – Line categories for managing the interface between load limits of vehicles and infrastructure*. Delft: NEN.
- Fenton, G.A., and Griffiths, D.V. 2008. *Risk Assessment in Geotechnical Engineering*. Hoboken: John Wiley & Sons, Inc.
- Fenton, G.A., and Vanmarcke, E.H. 1990. Simulation of random fields via local average subdivision. *Journal of Engineering Mechanics*, 116(8), pp.1733–1749.
- Hicks, M.A., and Li, Y. 2018. Influence of length effect on embankment slope reliability in 3D. *International Journal for Numerical and Analytical Methods in Geomechanics*, 42(7), pp.891–915.
- Hicks, M.A., Nuttall, J.D., and Chen, J. 2014. Influence of heterogeneity on 3D slope reliability and failure consequence. *Computers and Geotechnics*, 61, pp.198–208.
- Hicks, M.A., and Samy, K. 2002. Influence of heterogeneity on undrained clay slope stability. *Quarterly Journal of Engineering Geology and Hydrogeology*, 35(1), pp.41–49.
- Hicks, M.A., and Spencer, W.A. 2010. Influence of heterogeneity on the reliability and failure of a long 3D slope. *Computers and Geotechnics*, 37(7), pp.948–955.
- Phoon, K.-K., 2023. What geotechnical engineers want to know about reliability. *ASCE-ASME Journal of Risk and Uncertainty in Engineering Systems, Part A: Civil Engineering*, 9(2), pp.03123001-1–03123001-29.
- Salgado, R., Woo, S.I., and Kim, D. 2011. *Development of Load and Resistance Factor Design for Ultimate and Serviceability Limit States of Transportation Structure Foundations*. West Lafayette: Joint Transportation Research Program, Indiana Department of Transportation and Purdue University.
- Varkey, D., Hicks, M.A., and Vardon, P.J. 2023. Effect of uncertainties in geometry, inter-layer boundary and shear strength properties on the probabilistic stability of a 3D embankment slope. *Georisk: Assessment and Management of Risk for Engineered Systems and Geohazards*, 17(2), pp.262–276.